MgO/metal interfaces at low coverage: An order *N*, semiempirical Hartree-Fock simulation

C. Noguera,[1,2] J. Godet,[3] and J. Goniakowski[1,2]
[1]*CNRS, Institut des Nanosciences de Paris, UMR 7588, 140 rue de Lourmel, 75015 Paris, France*
[2]*UPMC–Université Paris 06, INSP, UMR 7588, 140 rue de Lourmel, 75015 Paris, France*
[3]*PhyMat, Physique des matériaux, Université de Poitiers, CNRS UMR 6630, Boulevard Marie et Pierre Curie SP2MI, Téléport 2, BP 30179, F-86962 Futuroscope Chasseneuil Cedex, France*
(Received 26 January 2010; revised manuscript received 4 March 2010; published 5 April 2010)

Thanks to the implementation of an order-*N* semiempirical Hartree-Fock method, which at the same time is accurate enough to allow a determination of electronic and structural properties of complex insulating systems with atoms in a wide range of environments, and is fast enough to tackle large size systems and repeated calculations, generic properties of monolayer and bilayer MgO square islands, deposited on a weakly interacting metal substrate, are studied. The presence of interfacial dislocations is evidenced, and their periodicity related to the two-dimensional lattice parameter of the unsupported islands. Two size regimes are identified: a small size regime, with no dislocations present (nanometric or subnanometric regime), in which edge effects play a prominent role and the island properties are driven by the small average coordination number of the atoms. At larger sizes, the properties present an oscillating behavior as a function of size, associated with the periodicity of interfacial dislocations. As regards electronic properties, their inhomogeneity inside the islands is expected to yield specific site reactivity or inhomogeneous surface potentials. Most stable islands are identified and their (magic) sizes have been related to the dislocation network periodicity, in agreement with existing experimental results for MgO on Ag(100) and Mo(100).

DOI: 10.1103/PhysRevB.81.155409 PACS number(s): 68.35.−p, 68.55.aj, 68.65.−k, 73.22.−f

I. INTRODUCTION

With the acceleration of device miniaturization, and the advances in synthesis and self-organization, it has become crucial to get a detailed understanding of the mechanisms which drive the formation of nano-objects. This is especially true for iono-covalent compounds such as oxides, which have been the subject of less studies than metals or semiconductors, despite the wide range of their potential applications, from optics to catalysis, spin electronics, etc.

In the last decade, efforts have concentrated on the fabrication of ultrathin oxide layers deposited on metal substrates.[1–5] It has been recognized that, in most cases, their properties largely differ from their bulk analogs, and may be tuned as a function of orientation, thickness, support characteristics, and stoichiometry. In addition, lateral confinement gives additional degrees of freedom for engineering artificial objects. Their interaction with a substrate raises questions related to epitaxial growth, formation of Moiré patterns, presence of interfacial dislocations, and elastic relaxation at the interfaces.[6,7] These effects are usually described within the framework of the elastic theory[8–10] or using very simplified models such as the Frenkel-Kontorova model.[11–14] However, the elastic approach is not well suited to nano-objects, since it neglects the discrete nature of the atomic structure. In this respect, atomistic simulations are a precious tool to complement it and enrich our understanding. The Frenkel-Kontorova model, on the other hand, was very useful in predicting, for example, the existence of solitonic solutions in a part of the interaction-misfit phase diagram. However, the underlying energetic model is oversimplified, with respect to what would be needed to describe complex systems such as oxide/metal interfaces and finite size effects are not easily handled.

However, if more realistic quantum simulations are mandatory, which has long been recognized to be the case for low-dimensional oxides,[15,16] the size of the simulated systems is strongly limited by the (usually) cubic scaling that most quantum codes display as a function of the number of atoms. Indeed, due to this limitation, in the physics of ultrathin oxide films, most simulations performed until now have assumed that the films adopt a perfect pseudomorphy with the substrate,[17] which is far from being the general case. To overcome the scaling problem, various approaches have been proposed, called "order-*N*" methods.[18–23] They rely on the idea that, in a given system, local properties can be computed from the knowledge of the electronic states just in the vicinity of the atoms under consideration. This idea has been conceptualized within the principle of "nearsightedness."[24] Some order-*N* methods are based on an orbital formulation of the electronic properties and others on the calculation of the Green's function or density matrix. We have adopted the latter and transformed the semiempirical Hartree-Fock type code that we used in the past,[25] so that it scales linearly with the size of the system. Such type of approach has mainly been used in the past for the description of large size organic or biological systems. Here it allows us to perform simulations necessary to tackle the complexity of the epitaxy of nano-oxides on metal surfaces, which is presently beyond the capabilities of full *ab initio* methods and has never been achieved, to our knowledge, at such level of quantum description.

In the present study, we simulate medium size systems, consisting in MgO islands of a few thousand atoms, deposited on a metallic substrate. Such nano-objects have been the subject of recent experimental works.[26–32] As a function of island size, we will discuss how the substrate influences their structural and electronic properties, and in particular the formation of interfacial dislocations. In relation with finite size

effects, we will consider the existence of magic islands, which present an enhanced stability. It is beyond the scope of this study to look in detail at equilibrium or growth shapes, which will be the subject of a forthcoming paper.[33] Nevertheless, considering that very few, if any, realistic simulations of oxide nano-objects on metal substrates have been performed until now, the limited scope of the present paper, which is to describe a generic case revealing the important parameters driving the characteristics of a complex interface, is already an advance with respect to existing works.

The paper is organized as follows: in Sec. II we recall the foundations of the semiempirical Hartree-Fock method, we show how linear scaling is obtained, we describe the methodology to obtain the parameter values necessary to its implementation in the case of MgO and the potential energy surface (PES) method used to account for the interaction with the substrate. In Sec. III, we analyze the structural and electronic properties of square MgO islands deposited on a metal substrate. Section IV is devoted to a discussion of our results in relation to recent experiments.

II. METHOD

After a short summary of the semiempirical Hartree-Fock formalism (Sec. II A), the principles of its transformation into an order-N method are described (Sec. II B), together with its performance as regards CPU time and memory (Sec. III C). Considering a simple oxide as MgO, we show how such a code, with parameters fitted to experimental data and *ab initio* calculations, can satisfactorily account for structural and energetic properties in a wide range of local environments (atomic coordination and geometry) (Sec. II D). Finally, in Sec. II E, we describe the implementation of a potential energy surface, which is used to represent the interaction of MgO islands with a metal substrate, in the limit of weak metal-oxide interaction.

A. Semiempirical Hartree-Fock method

The method relies on an effective restricted Hartree-Fock (RHF) variational method, in the Born-Oppenheimer approximation, in which the ground-state N-body electronic wave function is taken as a Slater determinant built from one-electron wave functions. The latter are expanded on an orthogonal atomic orbital minimal basis set $|A,a\rangle$ (a the atomic orbital on atom A). In the spirit of the INDO method,[34] only certain Fock matrix elements are kept: the overlap matrix, which is assumed to be unity, the diagonal and nondiagonal intra-atomic Coulomb and exchange terms g_{AaAb}, the two-center nondiagonal Coulomb terms g_{AB} (assumed independent of the orbitals involved), and finally the interatomic resonance integrals β_{AaBb} (one-electron intersite nondiagonal Fock terms). The general form of the Fock matrix elements as a function of the density matrix p is thus the following:

$$F_{AaAa} = \epsilon^0_{Aa} + \left(n_A - \frac{1}{2}p_{AaAa}\right)g_{AA} + \sum_{C\neq A}(n_C - n^0_C)g_{AC},$$

$$F_{AaAb} = -\frac{1}{2}p_{AaAb}g_{AA},$$

$$F_{AaBb} = \beta_{AaBb}. \quad (1)$$

In Eqs. (1), ϵ^0_{Aa} is the one-electron diagonal Fock term, n_A is the intra-atomic trace of the density matrix, and n^0_A is the number of valence electrons of the neutral A atom (opposite to its core charge). The last term in the expression of F_{AaAa} is the electrostatic potential due to the surrounding charges (Madelung potential in periodic systems).

Solving the Fock equations in a self-consistent manner with respect to the density matrix gives the electronic energy $E_{el}(\{\vec{R}_i\})$ function of the instantaneous position $\{\vec{R}_i\}$ of the ions. To obtain the total energy, a first-neighbor repulsion term E_{rep} has to be added,

$$E_{rep} = \frac{1}{2}\sum_{A\neq B}\frac{C_{AB}}{r^{q_{AB}}_{AB}}. \quad (2)$$

Its dependence upon the interatomic distances r_{ij} is driven by the exponent q_{ij}, which depends upon the type of ion pair under consideration. Forces on atoms are estimated thanks to the Helmann-Feynman theorem and ground-state structure may thus be determined by usual static or dynamic methods. Past studies have shown that such method is able to qualitatively and often quantitatively correctly account for electronic degrees of freedom in simple oxides and d^0 transition metal oxides.[25,35]

B. Order N implementation

The most time consuming part of the electronic structure calculation is the diagonalization of the Fock operator, which roughly scales as N^3 (N being the number of valence electrons in the system), and which has to be repeatedly performed until self-consistency is achieved. In order to transform the N^3 scaling into a linear scaling, we have adopted a "divide and conquer" strategy first introduced by Yang[36] for Kohn-Sham Hamiltonians and then generalized to Hartree-Fock and semiempirical calculations.[37,38] Thanks to the replacement of a large $M\times M$ matrix diagonalization (M being proportional to the size of the system) by a sequence of diagonalizations of smaller $(n\times n)$ matrices, the computational cost grows as $M\times n^3$ and linear scaling is achieved.

More specifically, the system is divided into overlapping clusters centered on each atom, which allow up to m electron hoppings (effective m neighboring shells). We construct and diagonalize the Fock matrix for each of these clusters and retain the local density of states (LDOS) on the central atoms only. The sum of the LDOS gives the total density of states, from which the Fermi level position is deduced, as well as the density matrix which is then used for the next self-consistency step.

The precision of the method is dependent upon the size m of the local clusters and increases with m. It can be shown that the LDOS calculated in that way have exact m first moments, as in recursion methods in which the continuous fractions which represents the diagonal elements of the Green's operator are truncated at the mth level.[15,39] The size of the clusters must always remain larger than the extension of one-electron wave functions. It is thus a method of choice for insulating systems, such as the low-dimensional oxides under consideration in the present study.

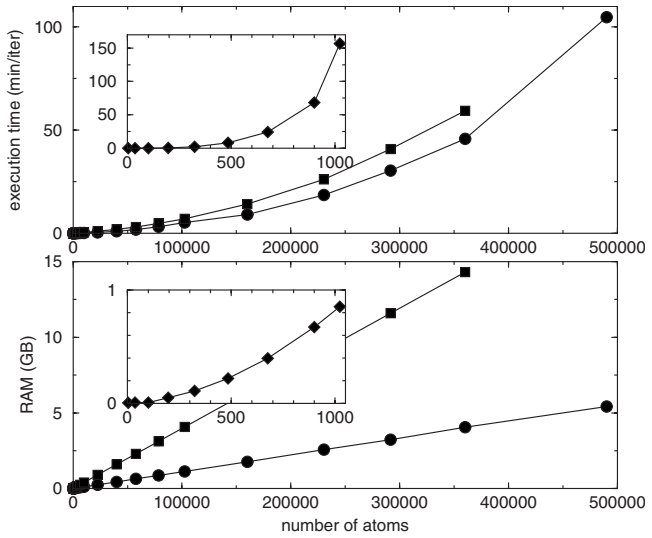

FIG. 1. Top panel: CPU time required for one iteration of electronic structure calculation, for MgO monolayer islands of increasing number of atoms: dots and squares correspond to the linear scaling implementation with local clusters containing $m=1$ and $m=2$ neighboring shells, respectively; in the inserts, results for the full diagonalization of the Fock operator. Note the different x axis scale. Lower panel: similar curves for the RAM.

C. CPU and memory performances

We have checked the computational performances of the method by recording the RAM and CPU time necessary for one iteration of electronic structure calculation of MgO monolayer islands of increasing sizes, on a scalar machine, with a single AMD Opteron processor.

The results are shown in Fig. 1. Indeed, both CPU and required RAM no longer grow as N^3. At the largest sizes, the scaling is not exactly linear, because of the electrostatic potential calculation which scales as N^2. This N^2 scaling could be improved, by using techniques such as the continuous fast multipole method;[40] the present work did not require it, due to the limited size of considered systems.

The gain of CPU time and memory is enormous: for an island of 100 000 atoms, 5–10 min per iteration ($m=1$ or 2 shells) and 4 Gigabytes RAM are necessary, to be compared to (extrapolated values) 100,000 years per iteration and 7 Terabytes RAM when full diagonalization is performed. In addition, we note that independent diagonalizations of $M(n \times n)$ matrices are suited for parallelization, a further increase of speed which is presently under development in our code.

D. Parametrization and fit quality

A part of the advantage of the semiempirical Hartree-Fock method lies in the fact that the two-center Fock matrix elements are not calculated by space integration of the Coulomb operator $1/|\vec{r}-\vec{r'}|$. Rather, the g_{AaBb} Coulomb terms in Eq. (1) are parameterized. While intra-atomic g_{AaAb} terms are taken as constant atomic characteristics, the interatomic g_{AB} terms are approximated using the Ohno-Kloppman formula[41]

$$g_{AB} = \frac{1}{\sqrt{r_{AB}^2 + D^2}} \tag{3}$$

in order to take into account the finite extension of the ionic charge distribution, in an effective way. The resonance integrals β_{AaBb} are the product of the Slater-Koster coefficients[42] $f(u_{\vec{AB}}, \eta_{AaBb})$—function of the unit vector $u_{\vec{AB}}$ which links the two atoms and of elementary overlap parameters η_i—by a distance dependence term that we take as an inverse power law,

$$\beta_{AaBb} = \frac{f(u_{\vec{AB}}, \eta_{AaBb})}{r_{AB}^{p_{AB}}} \tag{4}$$

for first-neighbor hopping or as an exponential term for hopping between second neighbor O-O atoms,

$$\beta_{AaBb} = f(u_{\vec{AB}}, \eta_{AaBb}) \exp(-p_{AB} r_{AB}) \tag{5}$$

In the case of MgO, keeping $2s$ and $2p$ orbitals for oxygen and $3s$ and $3p$ orbitals for magnesium, the total number of parameters required for the total energy calculations amounts to 22. Relying on knowledge gained in the past,[25,43] those 22 parameters are reduced to 10 by considering: (i) that the ϵ_s^0 and ϵ_p^0 for each atom conserve a constant difference; (ii) that the ratio between the η_{ij} may be considered as constant ($\eta_{ss}:\eta_{sp}:\eta_{pp\sigma}:\eta_{pp\pi}=1:-1:-1.4:0.4$); and (iii) that all g_{AaAb} values are equal (U_A values in the following) whatever a and b (CNDO approximation). In addition, the value of D in Eq. (3) is chosen such that the limit $r_{AB} \to 0$ of g_{AB} be equal to 10 eV.

In order to determine the values of these ten parameters, we fit a number of calculated observables to either experimental values or density-functional theory (DFT) *ab initio* results. Compared to an *ab initio* Hartree-Fock method, this step introduces effective values for the parameters (in particular, screened U values), allowing a better account of structural and electronic properties (e.g., bulk gap values closer to experiments). Since we wish the parametrization to account for a large range of geometries, with atoms displaying coordination numbers Z from 1 (the molecule) to 6 (rock-salt bulk), whether in periodic or nonperiodic arrangements, we consider the MgO molecule ($Z=1$), several small clusters: square Mg_2O_2 and hexagon Mg_3O_3 ($Z=2$), cube Mg_4O_4 ($Z=3$), unsupported two-dimensional layers of (111) ($Z=3$) or (100) ($Z=4$) orientations, and bulks in the zinc-blende ($Z=4$), h-BN ($Z=5$), and rock-salt ($Z=6$) structures. The *ab initio* results have been obtained using density-functional theory at the PW-91 gradient-corrected level,[44] as implemented in the Vienna *ab initio* simulation package code,[45] in which the interaction with core electrons is treated within the projected augmented wave method.[46]

The fitted parameters are reported in Table I and fit results are shown in Fig. 2. In principle, the parameter values depend upon the number of shells (m value) kept in the linear scaling algorithm. However, in the case of MgO, the variations are so weak that they can be neglected. It is found that the RHF method allows a fair account of the evolution of the important structural and energetic properties with the local environment of the atoms, as required for studies of complex

TABLE I. Values of the RHF parameters obtained from the fitting procedure. ϵ and U in eV; η in eV$\times$Å^p for first neighbors and in eV for second neighbors; p in Å^{-1} for O-O, C in eV$\times$Å^q.

Atoms	ϵ_s^0	ϵ_p^0	U
Oxygen	−40.4	−24.8	20.1
Magnesium	−5.0	15.1	3.9
β_{AaBb}	η_{ss}	p	
O-Mg	−0.641	1.55	
O-O	−14.84	1.59	
repulsion	C	q	
O-Mg	75.34	6.3	

systems. The transferability of the parameters is checked by comparing DFT and RHF results for unsupported periodic MgO (100) multilayers, shown in Fig. 3, which were not used in the fitting procedure. The evolution of lattice parameter and elastic property is very accurately reproduced, which is essential for the study described below.

E. Weak interaction with a metal substrate: PES approach

The principle of construction of the PES that we use to describe the interaction between the MgO islands and the substrate is reminiscent of the procedure used for the reverse system (metal on MgO substrate);[49] however the compound nature of MgO requires to modify it substantially.

The interaction is described as a sum of contributions from all atoms in the island. Each contribution depends on

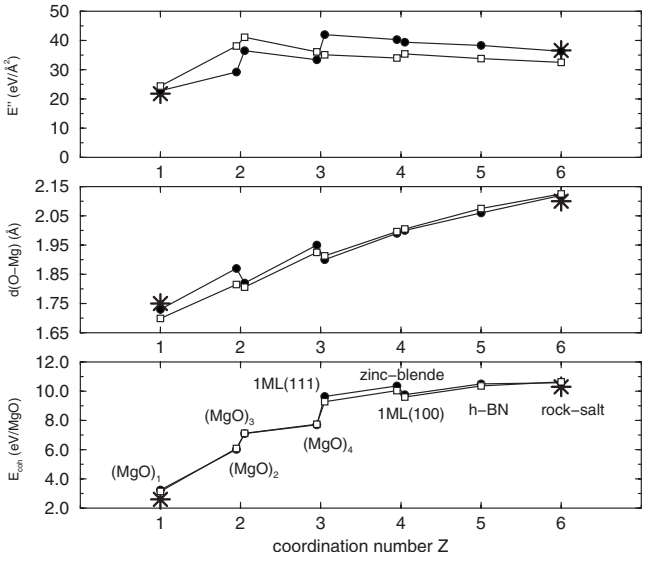

FIG. 2. Comparison between MgO properties calculated with DFT method (black dots) and RHF method with $m=2$ (squares), using the parameter values reported in Table I: Top panel: second derivative of the energy with respect to bond length; Middle panel: Mg-O bond length d; Lower panel: formation energy E_{coh} (with respect to neutral atoms). The systems under consideration are indicated in the lower panel (see text). Experimental results (stars) for MgO bulk and molecule are taken from Refs. 47 and 48.

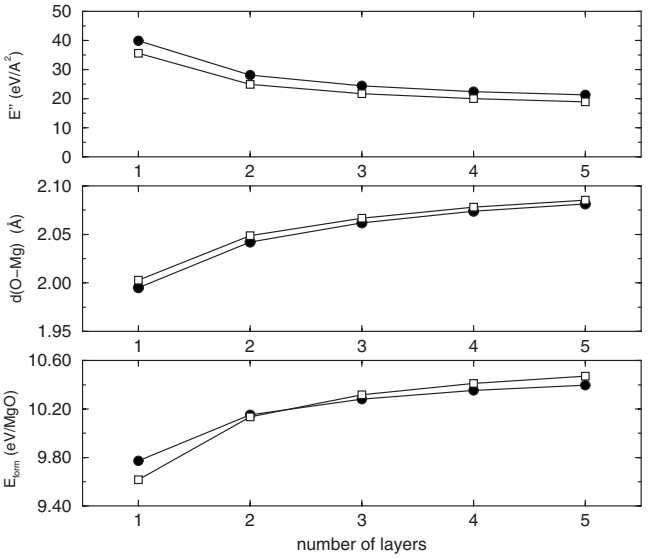

FIG. 3. Comparison between DFT (black dots) and RHF (squares) results, using the parameter values reported in Table I, for the description of unsupported infinite rocksalt (100) MgO layers of increasing thicknesses: Top panel: second derivative of the energy with respect to bond length; Middle panel: Mg-O bond length; Lower panel: formation energy E_{form} (with respect to neutral atoms).

the type at of atom involved [at_i=anion (A) or cation (C)] and on its horizontal (x_i and y_i) and vertical (z_i) position above the substrate

$$E^{sub} = \sum_{i=1}^{N} E_{int}^{at_i}(x_i, y_i, z_i). \tag{6}$$

For the metal substrate of square symmetry, we retain only the first terms in the Fourier expansion of the interaction potential [a the substrate two-dimensional (2D) lattice constant],

$$E_{int}^{at}(x,y,z) = b^{at}(z) + c^{at}(z)\left[\cos\left(\frac{2\pi x}{a}\right) + \cos\left(\frac{2\pi y}{a}\right)\right] + d^{at}(z)\left[\cos\left(\frac{2\pi(x+y)}{a}\right) + \cos\left(\frac{2\pi(x-y)}{a}\right)\right]. \tag{7}$$

For a given value of z and a given atom type at, the $b^{at}(z)$, $c^{at}(z)$, and $d^{at}(z)$ functions may be obtained, by linear combination, from the knowledge of interactions of atoms located at (lateral) high symmetry points with respect to the substrate: on-top (T), bridge (B), and hollow (H). At these high symmetry points, where the number of first-neighbor substrate atoms is well-defined (N_X=1, 2, and 4, respectively for $X=T$, B, H), the three functions $E_T^{at}(z)$, $E_B^{at}(z)$, and $E_H^{at}(z)$ are assumed to obey the same Morse-like law

$$E_X = N_X \lambda_1 [e^{-2\lambda_2(r-\lambda_3)} - 2e^{-\lambda_2(r-\lambda_3)}], \tag{8}$$

where r stands for the distance to the N_X first-neighbor substrate atoms (function of z and of the registry X).

In order to determine the coefficients λ_i for each type of atoms, three sets of independent periodic *ab initio* calcula-

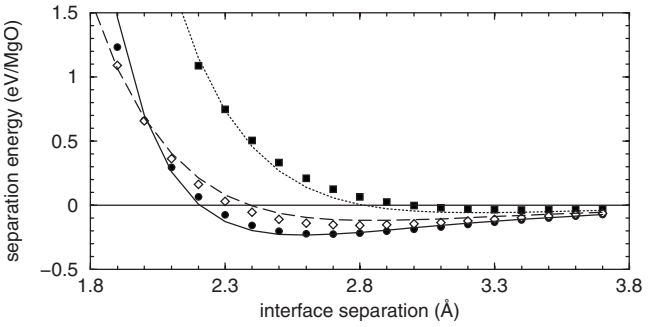

FIG. 4. Dependence of the separation energy of an MgO monolayer deposited on Ag(001) on the interface separation. Three registries are considered: oxygen on-top (dots); oxygen on-bridge (diamonds) and oxygens in hollow sites (squares). The symbols display the results of *ab initio* calculations and the lines the PES fit with parameters given in the text.

tions of MgO layers deposited on the substrate, with a constrained pseudomorphy but otherwise full atomic relaxation, are performed, corresponding to three different registries compatible with the (001) island structure: in the first one, anions are on-top substrate atoms and cations in hollow sites $E_1(z)=E_T^A(z)+E_H^C(z)$; in the second, anions and cations are in bridge sites: $E_2(z)=E_B^A(z)+E_B^C(z)$; in the third one, anions are in hollow sites and cations on-top: $E_3(z)=E_H^A(z)+E_T^C(z)$. Dense scan in z is performed numerically to increase the fit quality.

The whole PES is thus fitted with only six parameters (three for each type of atoms). Figure 4 shows the quality of the fit attainable in the case of MgO monolayers on Ag(001), at the Ag equilibrium lateral lattice parameter, with the following set of parameters: $\lambda_i=0.136$ eV, 2.331 Å^{-1}, 2.464 Å for oxygen and $\lambda_i=0.042$ eV, 1.589 Å^{-1}, 3.383 Å for magnesium ($i=1$ to 3). The equilibrium interface distance of 2.60 Å for O-top registry, is in agreement with previous calculations made with the same method,[27] and is slightly larger than experimental estimations.[27,29] We note that such formulation of PES enables an efficient determination of E^{sub} for any low-symmetry position of atoms, without additional hypothesis on the number of nearest neighbors. It is reminiscent of the interaction present in the Frenkel-Kontorova model, but it additionally includes a z dependence (allowing tilt and rumpling) and can be used for compound islands (with two or more types of atoms). On the other hand, charge transfer and other quantum interactions between islands and substrate[50,51] are not included in the PES description.

III. PROPERTIES OF MGO SQUARE ISLANDS ON A METAL SUBSTRATE

We have applied the above methodology to the simulation of model square MgO islands deposited on a metallic substrate, in the limit of a weak interaction represented by a PES. In the present study, we focus on structural and electronic characteristics induced by the substrate, leaving the question of its influence on the island shape to a future work. For this reason, a simple square shape is chosen. We discuss the structural (Sec. III A) and electronic (Sec. III B) properties of large monolayer and bilayer islands of fixed size, and, in Sec. III C, we analyze how these properties evolve as a function of size.

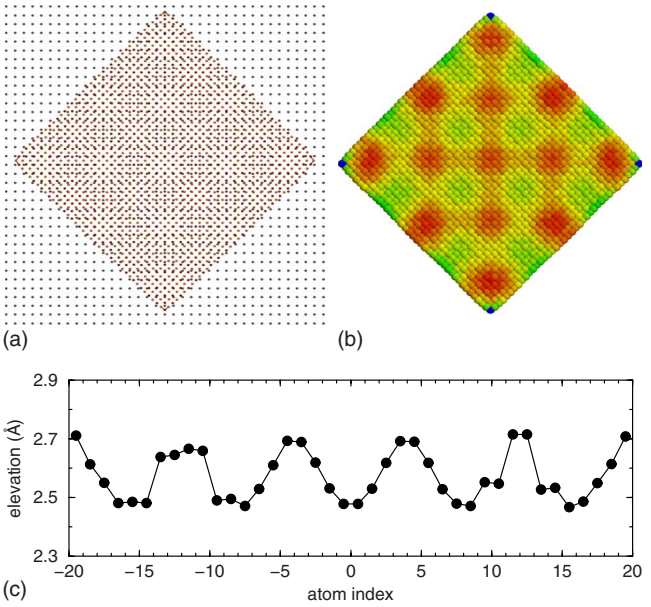

FIG. 5. (Color online) Top left panel: Structure of an MgO(100) island of 1600 atoms deposited on a metal substrate. Gray, red (dark), and yellow (light) dots represent substrate, oxygen and magnesium atoms, respectively. Top right panel: color representation of the mean Mg-O distance $\langle d_{\text{Mg-O}}\rangle$ around each atom. Larger to smaller $\langle d_{\text{Mg-O}}\rangle$ from red to green (from dark to light gray). Lower panel: vertical position profiles along the island diagonal.

A. Structural properties of monolayer and bilayer islands

In the following, we discuss the structure of MgO monolayer (1 ML) and bilayer (2 ML) square islands made of 1600 and 3200 atoms, respectively, deposited on a generic metal substrate with a lattice parameter equal to $a=3.2$ Å, and an interaction strength equal to twice that with the Ag substrate. Aside from the square geometry constraint, full optimization of all structural degrees of freedom is performed until forces are less than 10^{-3} eV/Å.

A typical 1 ML MgO island structure is shown in Fig. 5 (top left panel). The island edges are nonpolar with alternating oxygen and magnesium atoms. Rows of a single type of ions run parallel to the dense atomic rows of the substrate surface [x (horizontal) and y (vertical) axes]. A Moiré pattern is evidenced with zones of coincidence and anticoincidence. It is due to the misfit between the MgO layer and the substrate lattice parameters, the former being smaller than the latter. The island edges remain quasilinear, although somewhat distorted and some rounding occurs at the corners. This latter feature is also found in unsupported islands.

Local distortions of the MgO lattice occur upon deposition. They are evidenced in Figs. 5 and 6 for 1 ML and 2 ML islands, respectively. The maps display the mean Mg-O bond length around each atom, in a color scale. It shows that bond expansion takes place in the coincidence zones (in particular at the island center where an oxygen atom is located on-top

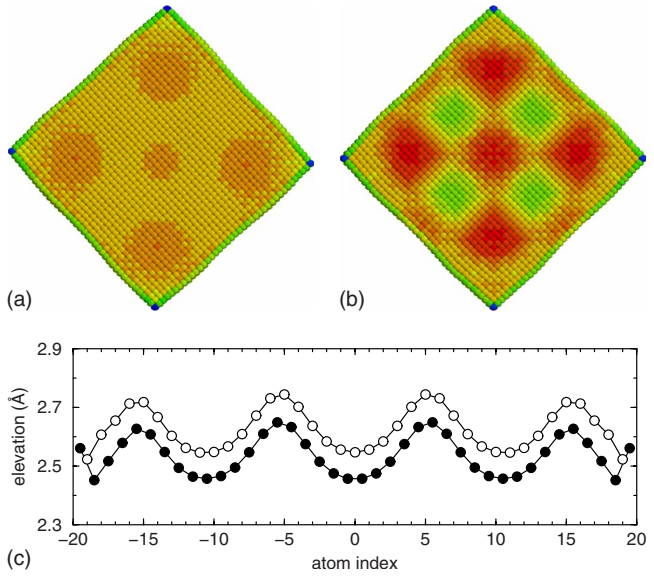

FIG. 6. (Color online) Top panel: Color representation of the mean Mg-O distance $\langle d_{\text{Mg-O}} \rangle$ around each atom in a 3200-atom MgO bilayer (left: surface layer; right: interfacial layer). Same colors as in Fig. 5. Lower panel: vertical displacement profiles along the x axis. Black dots: interface atoms; open dots: surface atoms

a substrate atom) while bond contraction occurs in the anticoincidence zones, where Mg atoms are located on-top substrate atoms. The modulation is smaller at the surface of the 2 ML island than in the interfacial layer, consistently with the fact that the forces exerted by the substrate are smaller. The lower panel of Fig. 5 shows that, additionally, the layers are tilted in the dislocated zones. The tilt angle is of the order of 2° and 1° in monolayer and bilayers, respectively. Some rumpling also occurs in the anticoincidence zones.

The in-plane atom positions x_n display three main features: (i) a periodicity associated to a mean lattice parameter, $\bar{a}=\gamma a$, different from the substrate lattice parameter a, (ii) a periodic modulation, and (iii) additional displacements δx_n close to the edges,

$$x_n = n\gamma a + a\alpha \sin 2\pi n(1-\gamma) + \delta x_n, \tag{9}$$

with n the atom index ($n=0$ at the island center). Figure 7 shows how the analysis of this quantity proceeds for the 1 ML island. In the top panel, $x_n/a-n$ is plotted as a function of n. If the island lattice were in pseudomorphy with the substrate ($\gamma=1$), this quantity would be zero. In the 1 ML island, a quasilinear slope is found, which corresponds to $\gamma \approx .875$. It allows to identify a commensurability locking at a value close to $\gamma=7/8$. The sinusoidal modulation, shown in Fig. 7 middle panel, is characterized by a periodicity $n=8$, consistent with the γ value and with the local periodic distortions displayed in Fig. 5. It can easily be understood from the consideration of the local forces exerted by the substrate. In the central part of the island (see Fig. 7 middle panel), the modulation reproduces that found in an infinite 1 ML MgO film deposited on the metal substrate with the same commensurability locking, obtained in a periodic calculation. The edge contribution δx_n is localized on the four to five atoms

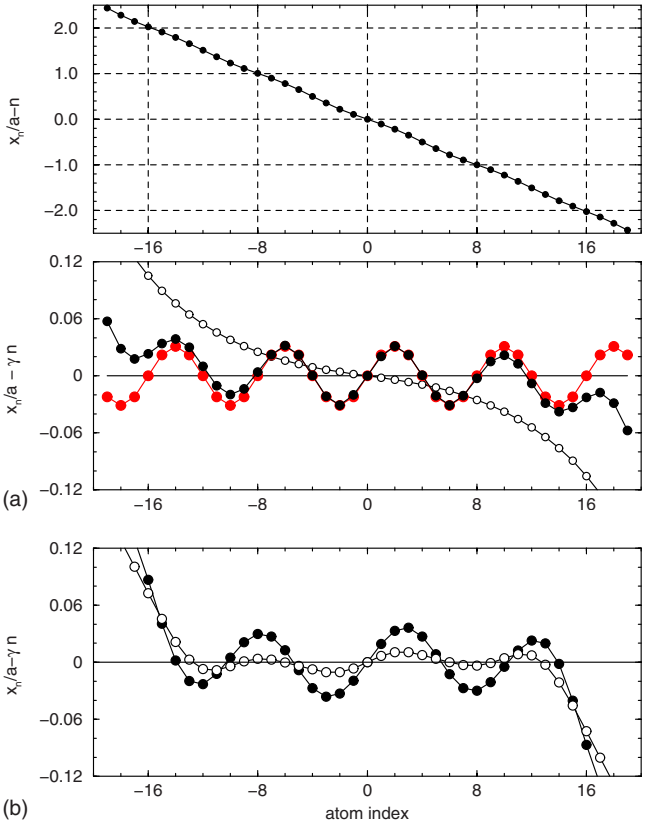

FIG. 7. (Color online) Analysis of the atom positions along the x axis in a 1600 atom 1 ML MgO island as a function of the atom index n. Top panel: $x_n/a-n$; Middle panel $x_n/a-7n/8$; black and red (gray) dots represent this quantity for the island and for the infinite monolayer with the same commensurability locking, respectively; open sysmbols are for an unsupported 1600-atom island. Lower panel: $x_n/a-19n/21$ for the 2 ML island; full and empty symbols for the interface and surface atoms, respectively

from the island edges. It corresponds to a lattice contraction around undercoordinated atoms. It is more localized than in unsupported islands where the penetration length is of the order of ten interatomic distances (Fig. 7 middle panel).

In the 2 ML MgO island, the position analysis proceeds in a similar way (Fig. 7 lower panel). Both for atoms at the interface with the substrate and at the island surface, the slope of $x_n/a-n$ and the sinusoid period are consistent with $\gamma=0.905$, a value close to 19/21. The α coefficient in front of the sine function in Eq. (9) is larger for interface than for surface atoms.

The dislocation network lattice parameter A may be inferred from the $(a-\bar{a})$ misfit between the substrate and the deposited island. Recalling the notation $\bar{a}=\gamma a$, it reads

$$A = \frac{\gamma}{(1-\gamma)}a. \tag{10}$$

This estimation yields $A=22.3$ Å for 1 ML and $A=30.5$ Å for 2 ML, in perfect agreement with calculated values.

B. Electronic properties of monolayer and bilayer islands

The advantage of the RHF quantum mechanical treatment lies in the fact that it yields at the same time structural and electronic information.

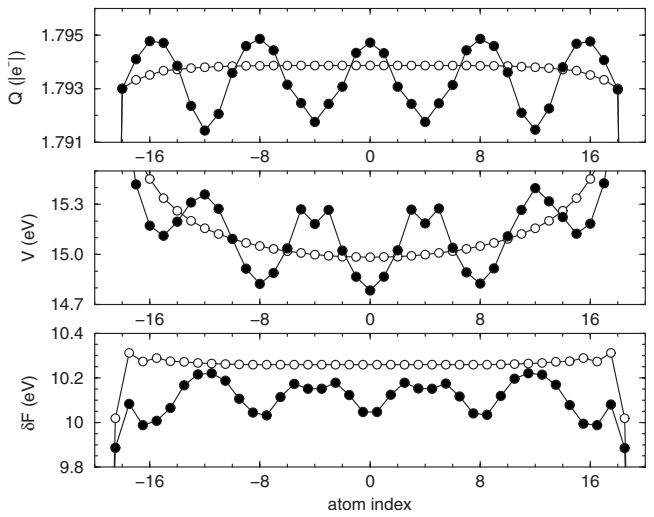

FIG. 8. Local electronic property profiles along the x axis for an 1600 atom MgO monolayer island: Top panel: charges Q (absolute values); Middle panel: electrostatic potential V on oxygen atoms; Lower panel: difference in effective level positions on neighboring cation and anion $\delta F = F_{\mathrm{Mg}s\mathrm{Mg}s} - F_{\mathrm{O}p_z\mathrm{O}p_z}$ (see text). Empty and black symbols are for unsupported and supported islands, respectively

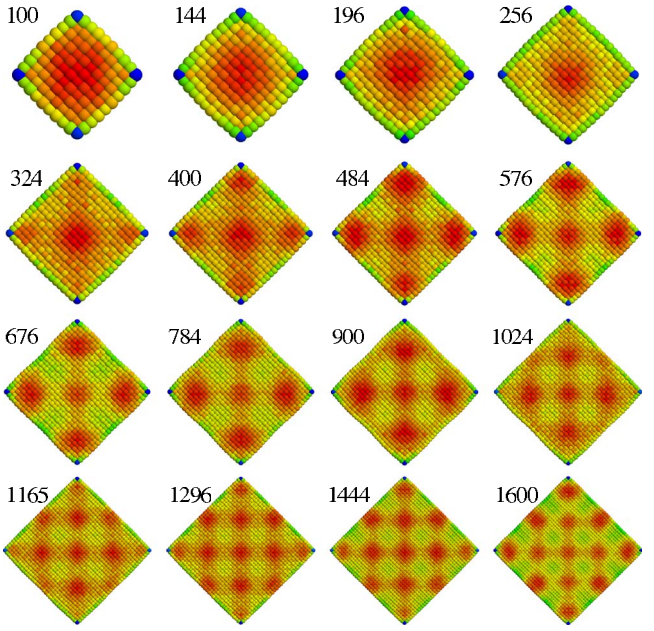

FIG. 9. (Color online) Color representation of the mean Mg-O distance around each atom $\langle d_{\mathrm{Mg\text{-}O}} \rangle$ in 1 ML MgO islands of increasing sizes. Same color representation as in Fig. 5. For the sake of visibility, all islands are shown with the same area, whatever their atom number

As a function of the atom index n, Fig. 8 represents the profiles of ionic charges $|Q|$, local electrostatic potential (in absolute value) V, and difference in effective level positions on neighboring cation and anion $\delta F = F_{\mathrm{Mg}s\mathrm{Mg}s} - F_{\mathrm{O}p_z\mathrm{O}p_z}$, along the x axis for the 1 ML island ($N=1600$ atoms). The latter quantity is indicative of the gap value G, but since it neglects band width effects, it usually overestimates G. Only its size variations will be discussed in the following. Aside from edge effects, all electronic quantities present a flat profile in unsupported islands, while they are modulated, albeit weakly for some of them, in supported islands, with a periodicity consistent with the structural effects discussed above. As already pointed out in Sec. III A, bonds are elongated in the coincidence zones, due to the smaller lattice parameter of the MgO islands, compared to the substrate. Their maxima are associated to minima (in absolute value) of the electrostatic potential, to maxima of charges and to minima of δF. These findings may be easily rationalized in the following way: far from the edges, in the coincidence zones, atoms are further apart and they exert a smaller electrostatic potential on each other. This trend, found on oxygen atoms, is less obvious on magnesium atoms, but the overall effect on δF turns out to be driven by the oxygens. Aside from Madelung potential effects, the modulation of δF contains a contribution from intra-atomic electron-electron repulsion which opposes the Madelung variation. This partial cancelation is well known when one considers the intra-atomic and interatomic electrostatic contributions to the dielectric constants of insulators.[15] Finally, the charge variations are very weak, because the oxygen-magnesium electron sharing is a function of the ratio between resonance integrals and the anion-cation effective orbital energy difference δF.[15] While the numerator decreases with bond-length elongation, the denominator also decreases because δF decreases. A partial cancelation thus occurs, the resulting effect being driven by δF. In the 2 ML island, similar effects are observed, with smaller modulations in the surface than in the interface layer.

Edge effects also reflect themselves in the electronic properties. The bond shortening and reduction of coordination number are reflected in a decrease of charge and δF.

C. Size evolution of island properties and existence of magic islands

In the previous subsections, we have analyzed the local structural and electronic properties of large 1 ML and 2 ML islands of fixed size (1600 and 3200 atoms, respectively). We now discuss more global properties, in order to understand how the islands as a whole respond to the substrate interaction as a function of their size.

In the present case, we find that the value of the commensurability parameter γ [Eq. (9)] presents only weak variations with the island size, around the values $7/8=.875$ and $19/21=.9048$, for 1 ML and 2 ML islands, respectively. The associated dislocation network lattice parameters are thus of the order of 22.4 Å, and 30.5 Å, respectively. For the monolayer, the centers of the interfacial dislocations are located at atom indices $n=\pm(4+8k)$ (k an integer). They should thus appear at island sizes such that the corner atoms have these indices, which corresponds to islands of sizes equal to $N=100$, 676, 1764, etc. For 2 ML, corresponding sizes are $N=288$, 2048, etc. According to Fig. 9, which displays local Mg-O bond-length maps of 1 ML MgO islands at increasing sizes from $N=100$ to $N=1600$, it turns out that, while the periodicity of this effect is well predicted, edge effects somewhat blur the appearance of new interfacial dislocations.

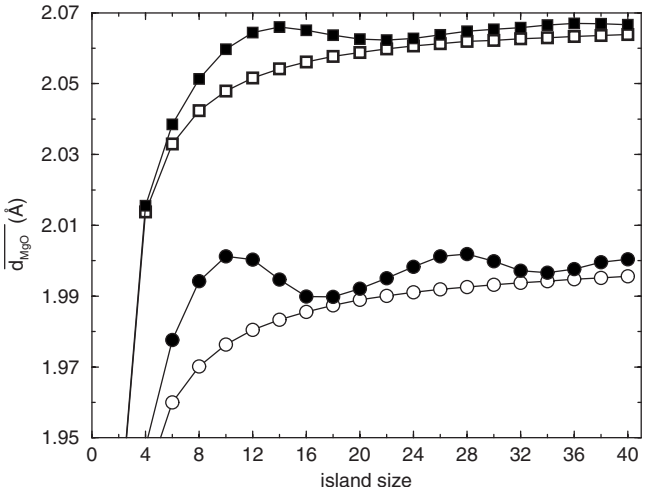

FIG. 10. Evolution of the average Mg-O distance $\overline{d_{MgO}}$ in the whole islands as a function of size in 1 ML and 2 ML MgO islands. Black dots and squares for supported 1 ML and 2 ML islands, respectively; white symbols for corresponding flat unsupported layers. The x scale represents $\sqrt{N}$ and $\sqrt{N/2}$ for 1 ML and 2 ML, respectively.

As an example of global structural property, we consider the mean Mg-O distance value d_{MgO}, averaged over the whole islands, as represented in Fig. 10 for 1 ML and 2 ML of increasing sizes. A (sub)-nanometer regime is clearly seen ($N<100$ and $N<392$ for 1 ML and 2 ML, respectively, which correspond to $\sqrt{N}=10$ and $\sqrt{N/2}=14$, respectively), in which the reduction of the coordination number for a large number of atoms is responsible for a very low value of d_{MgO}. At larger sizes, this quantity presents oscillations as a function of size. Well defined maxima occur at $N=100$ and $N=784$ for 1 ML ($\sqrt{N}$ equal to 10 and 28) and at $N=392$ and $N=2592$ for 2 ML ($\sqrt{N/2}$ equal to 14 and 36). The same is true (not shown) for the mean Mg-O distance at the center of the islands, and for the electronic properties (with inversion between maxima and minima, with respect to d_{MgO}, in agreement with the considerations given in Sec. III B). These characteristic sizes are close to the sizes at which new dislocations are introduced.

As regards edge effects, Fig. 11 shows the vertical and horizontal displacements of the corner atoms as a function of island size. They display oscillations due to their periodic change of registry with the substrate. It turns out that for some sizes, the amplitude of the oscillations is larger than at

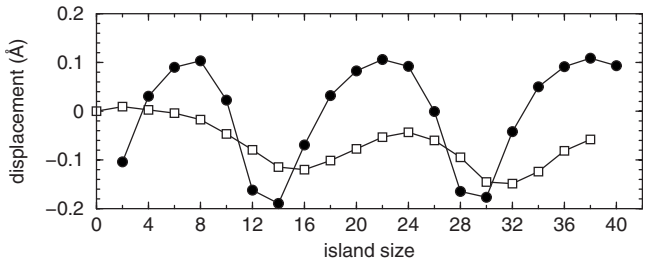

FIG. 11. Evolution of the horizontal (open squares) and vertical (dots) displacement of corner atoms as a function of island size ($\sqrt{N}$) in 1 ML MgO islands.

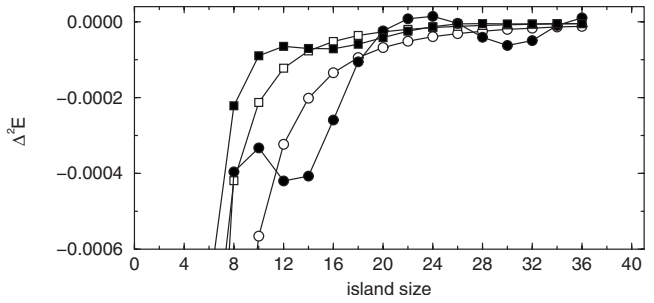

FIG. 12. Energy second difference with respect to island size (in eV). Black dots and squares for 1 ML and 2 ML islands, respectively. Open symbols for flat unsupported islands. The x scale represents $\sqrt{N}$ and $\sqrt{N/2}$ for 1 ML and 2 ML, respectively

the island center (also seen in Fig. 7 middle panel). This may be assigned to the undercoordination of the edge atoms, which allows them to respond to external forces with more flexibility.

Another manifestation of finite size effects is the enhanced stability of supported islands at some (magic) sizes. This phenomenon, referred to as "magicity" has been the subject of numerous detailed studies in the physics of free clusters[52] and has also been scrutinized for the reverse system: metallic clusters deposited on MgO surfaces.[49,53] If estimated with respect to attachment and detachment of monomeric units, the condition on the size dependence of the energy $E(N)$ of a magic cluster is that its second difference with respect to N, $\Delta^2E=E(N+1)+E(N-1)-2E(N)$, be positive.

Adapted to the square islands considered here, we keep in mind that only certain types of detachment are accounted for and that the precision is lower at smaller sizes. In Fig. 12, Δ^2E is plotted as a function of $\sqrt{N}$ for 1 ML and $\sqrt{N/2}$ for 2 ML islands, both for supported and flat unsupported MgO islands. While it displays a monotonic behavior in the latter case, two distinct maxima at $N_1=100$ and $N_2=576$ and the hint of a third one at $N_3>\sim 1600$ are visible when supported monolayer islands are considered. Δ^2E is negative at N_1 and slightly positive at N_2. For bilayer islands, one maximum occurs at $N_1=288$ ($\sqrt{N/2}=12$) and two weak maxima may be found at $N_2=1568$ and $N_3=2312$ ($\sqrt{N/2}=28$ and 34, respectively). These values of the magic sizes are just inferior to those at which new interfacial dislocations appear (see above).

Magic sizes may be qualitatively understood with a simple argument. When a dislocation is introduced, edge atoms are located at energetically unfavorable positions with respect to substrate atoms. Since the direct interaction with the substrate represents the largest contribution to the total adhesion energy (in the present case, the distortion energy is less than a few percents), the overall stability of the islands thus decreases. The magic sizes should thus directly precede those at which dislocations are introduced. This criterion does not provide exact values because, as mentioned above, edge effects somewhat blur the introduction of dislocations. However, it represents a good guideline. In particular, it allows predicting the size N_1 and the edge length L_1 characteristic of the smallest 1 ML magic clusters,

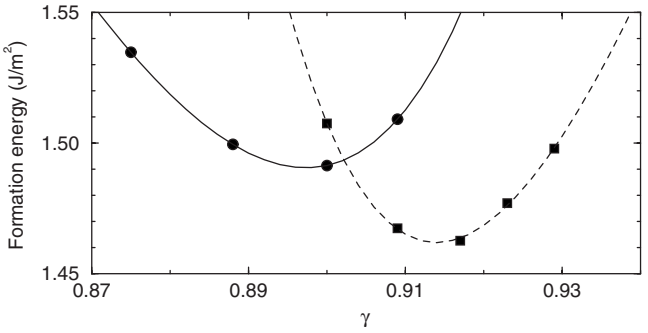

FIG. 13. Formation energy of periodic 1 ML (full line) and 2 ML (dashed line) films as a function of commensurability parameter γ.

$$N_1 = \frac{1}{(1-\gamma)^2}; \quad L_1 = \frac{\gamma a}{\sqrt{2}(1-\gamma)} = \frac{A}{\sqrt{2}}. \tag{11}$$

Subsequent magic islands occur at $N_k=(2k-1)^2*N_1$ and $L_k=(2k-1)*L_1$. For 2 ML magic clusters, identical formula apply for L_1 and L_2, while numbers of atoms should be doubled. These formula give $N_1=64$ and $N_2=576$ for 1 ML islands and $N_1=221$ and $N_2=1994$ for 2 ML. They thus somewhat underestimate the N_1 values, likely because they do not take into account edge effects, while they give a fair estimation of N_2.

IV. DISCUSSION

From the results presented in the preceding sections, it is clear that none of the islands that we have simulated is pseudomorphic with the substrate, which would correspond to a commensurability parameter γ equal to 1. Conversely their structure and properties display a clear relationship with their lattice misfit with the substrate $(\bar{a}-a)/a$. However predicting the value of $\bar{a}$ is by no means simple, since it depends on the characteristics of the unsupported islands and on their interaction with the substrate.

Indeed, on the one hand, $\bar{a}$ is far from being equal to the bulk MgO value $a_B=2.998$ Å, because bulk atoms are sixfold coordinated. A smaller value a_F is expected for unsupported periodic 1 ML and 2 ML films, which have a large proportion of fourfold and fivefold coordinated atoms, respectively. Indeed, Fig. 3 shows that a_F strongly varies with the layer thickness, from 2.832 Å at 1 ML to 2.897 Å at 2 ML. However, the ground state for supported 1 ML and 2 ML periodic films is not determined by a_F. We have performed additional simulations for these infinite films in 2D unit cells of different sizes, corresponding to different values of the commensurability parameter γ. As shown in Fig. 13, the ground state is found for values $\overline{a_F}$ slightly larger than a_F: 2.871 and 2.925 Å associated to extrapolated $\gamma=\overline{a_F}/a$ values 0.8973 and 0.914, for 1 ML and 2 ML, respectively.

In addition, in finite size unsupported islands, edge effects induce a strong reduction of bond lengths around edge and corner atoms, whose penetration is such that the lattice parameter at the island center a_I varies with size in a nonnegligible manner. Considering a_I values at the (finite size) island center, the ratio a_I/a turns out to be close to the $\gamma=\bar{a}/a$ values obtained in the simulation. For the present system, we thus find that the following equality is approximately obeyed:

$$\bar{a} \approx a_I. \tag{12}$$

The understanding gained in this study allows rationalizing some results which have been obtained experimentally. One such system concerns MgO islands on an Ag(100) substrate. Reflection high energy electron diffraction (RHEED) measurements,[28] have evidenced how the mean lateral lattice parameter $\bar{a}$ of the films increases with thickness. At 1 ML, it is close to the Ag substrate value $a_{Ag}=2.892$ Å, while the bulk MgO value is recovered at larger thicknesses. In reference, our calculated value $a_F=2.832$ Å at 1 ML is also very close to a_{Ag}. This would imply quasi-pseudomorphy between the monolayer and the substrate. However, magic clusters have been observed by STM with sizes of $L_1 \approx 70$ Å in the subnanometer regime[26] or 70 ± 20 Å.[32] If magicity is related to interfacial dislocations, according to the relationship Eq. (11) between L_1, the dislocation network lattice parameter A, and the commensurability parameter γ, one would rather deduce that $\bar{a}=2.810$ Å at 1 ML. The small difference between this value and that found by RHEED might come from the fact that, in the experiment, MgO does not exactly grow in a layer-by-layer fashion. The contribution of some thicker domains of the film may lead to a slight overestimation of the lattice parameter in the thinnest films.

In the presence of interfacial dislocations, one would expect the Moiré pattern to have been experimentally observed. To our knowledge, this has not been the case for MgO/Ag(100), but a recent work on MgO/Mo(100) (Ref. 31) has demonstrated that special bias conditions, corresponding to field emission resonances, are required for such an observation. The authors of Ref. 31 evidence 1 ML islands which are quite uniform in size and orientation, with apparent lateral size of 55 Å. In a grazing incidence x-ray diffraction (GIXD) (Ref. 30) study, the lateral lattice parameter of the layers was determined, $\bar{a}=3.03$ and 3.02 Å for 1 ML and 2 ML [Fig. 1b of Ref. 30] and the dislocation network lattice parameter A was shown to be consistent with these values. Additionally, using, Eq. (11), it is also consistent with the apparent magic size $L_1=55$ Å, found by STM.[31] We note that, contrary to the present study, the $\bar{a}$ value issued from GIXD, is far from being equal to a_I. We will argue in a forthcoming paper[33] that Eq. (12) is only valid in the limit of weak interactions of the islands with the substrate. As the interaction strength increases, γ should also increase, eventually leading to pseudomorphy ($\gamma=1$). The formation of strong interfacial oxygen-molybdenum bonds certainly places the MgO/Mo(100) interface in the strongly interacting regime.

Finally, we note that electronic properties are highly inhomogeneous in the islands, which could result in specific spectroscopic features, visible in scanning probe microscopy/spectroscopy: shift of the band edges or modulation of the surface potential. They may also result in specific adsorption properties, driven by changes in the donor or acceptor character of the island atoms.

V. CONCLUSION

We have implemented an order-*N* semiempirical Hartree-Fock method, which at the same time is accurate enough to allow a determination of electronic and structural properties of complex insulating systems with atoms in a wide range of environments, and is fast enough to tackle large size systems and repeated calculations. We have shown that this method allows a huge gain of CPU time and RAM compared to diagonalization of the full Fock matrix, while properties of MgO from the molecule to the bulk can well be reproduced. Such type of approach has mainly been used in the past for the description of large size organic or biological systems. Here, associated with the construction of a potential energy surface to describe a weak interaction with a substrate, it allows us to tackle the complexity of the epitaxy of nano-oxides on metal surfaces. Such a study would be presently beyond the capabilities of full *ab initio* methods. This represents a strong improvement with respect to other methods (elasticity theory, Frenkel-Kontorova models), which are presently applied to such systems, since it allows to take into account electronic degrees of freedom, defects, etc.

We have used this method to study the generic properties of monolayer and bilayer MgO square islands, deposited on a metal substrate in the limit of weak interaction. Interfacial dislocations have been identified, and their periodicity related to the 2D lattice parameter of the supported islands. We have identified two size regimes: a small size regime, with no dislocations present (nanometric or subnanometric regime), in which edge effects play a prominent role and the island properties are driven by the fact that the average coordination number of the atoms is small. At larger sizes, the properties present an oscillating behavior as a function of size, associated with the periodic introduction of interfacial dislocations. As regards electronic properties, their inhomogeneity inside the islands is expected to be associated to specific site reactivity or inhomogeneous surface potentials. We have found that there exist magic sizes for the supported islands. We have related their sizes to the dislocation network periodicity, in agreement with experimental results obtained for MgO on Ag(100) and Mo(100).

ACKNOWLEDGMENTS

Support of the French ANR-PNANO 2006 (project "SIMINOX" 0039) is acknowledged. Julien Godet acknowledges a post-doctoral support at the INSP during the first stages of this work. We also thank L. Jeloaica for some tests during this same period. We are grateful to G. Cabailh, R. Lazzari, J. Jupille, and N. Nilius for communication of their experimental results prior to publication.

[1] E. Lundgren, A. Mikkelsen, J. N. Andersen, G. Kresse, M. Schmid, and M. P. Varga, J. Phys.: Condens. Matter **18**, R481 (2006).
[2] H. J. Freund, Surf. Sci. **601**, 1438 (2007).
[3] C. Freysoldt, P. Rinke, and M. Scheffler, Phys. Rev. Lett. **99**, 086101 (2007).
[4] H. J. Freund and G. Pacchioni, Chem. Soc. Rev. **37**, 2224 (2008).
[5] S. Surnev, F. Allegretti, and F. P. Netzer, J. Vac. Sci. Technol. B **28**, 1 (2010).
[6] J. H. Van der Merwe, Surf. Sci. **31**, 198 (1972).
[7] I. Markov and S. Stoyanov, J. Contemp. Phys. **28**, 267 (1987).
[8] R. Kern and P. Muller, Surf. Sci. **392**, 103 (1997).
[9] A. Bourret, Surf. Sci. **432**, 37 (1999).
[10] P. Muller and A. Saul, Surf. Sci. Rep. **54**, 157 (2004).
[11] J. Frenkel and T. Kontorova, J. Phys. (USSR) **1**, 137 (1939).
[12] F. C. Frank, J. H. Van der Merwe, Proc. R. Soc. London **198**, 205 (1949); **198**, 216 (1949).
[13] G. Theodorou and T. M. Rice, Phys. Rev. B **18**, 2840 (1978).
[14] P. Bak, Rep. Prog. Phys. **45**, 587 (1982).
[15] C. Noguera, *Physics and Chemistry at Oxide Surfaces* (Cambridge University Press, Cambridge, 1996).
[16] T. Albaret, F. Finocchi, and C. Noguera, Faraday Discuss. **114**, 285 (1999).
[17] B. D. Yu and J. S. Kim, Phys. Rev. B **73**, 125408 (2006).
[18] P. Ordejón, Comput. Mater. Sci. **12**, 157 (1998).
[19] S. Goedecker, Rev. Mod. Phys. **71**, 1085 (1999).
[20] G. Galli, Phys. Status Solidi B **217**, 231 (2000).
[21] S. Y. Wu and C. S. Jayanthi, Phys. Rep. **358**, 1 (2002).
[22] M. J. Gillan, D. R. Bowler, A. S. Torralba, and T. Miyazaki, Comput. Phys. Commun. **177**, 14 (2007).
[23] P. Ordejón, Phys. Status Solidi B **217**, 335 (2000).
[24] W. Kohn, Phys. Rev. Lett. **76**, 3168 (1996).
[25] J. Goniakowski, S. Bouette-Russo, and C. Noguera, Surf. Sci. **284**, 315 (1993).
[26] S. Schintke, S. Messerli, M. Pivetta, F. Patthey, L. Libioulle, M. Stengel, A. De Vita, and W. D. Schneider, Phys. Rev. Lett. **87**, 276801 (2001).
[27] C. Giovanardi, A. di Bona, T. S. Moia, S. Valeri, C. Pisani, M. Sgroi, and M. Busso, Surf. Sci. **505**, L209 (2002).
[28] M. Kiguchi, T. Goto, K. Saiki, T. Sasaki, Y. Iwasawa, and A. Koma, Surf. Sci. **512**, 97 (2002).
[29] P. Luches, S. D'Addato, S. Valeri, E. Groppo, C. Prestipino, C. Lamberti, and F. Boscherini, Phys. Rev. B **69**, 045412 (2004).
[30] S. Benedetti, P. Torelli, S. Valeri, H. M. Benia, N. Nilius, and G. Renaud, Phys. Rev. B **78**, 195411 (2008).
[31] H. M. Benia, P. Myrach, N. Nilius, and H.-J. Freund, Surf. Sci. **604**, 435 (2010).
[32] G. Cabailh, R. Lazzari, and J. Jupille, private communication.
[33] J. Goniakowski, C. Noguera (unpublished).
[34] J. A. Pople, D. P. Santry, and G. A. Segal, J. Chem. Phys. **43**, S129 (1965).
[35] A. Pojani, F. Finocchi, and C. Noguera, Surf. Sci. **442**, 179 (1999).
[36] W. Yang, Phys. Rev. Lett. **66**, 1438 (1991).
[37] T. S. Lee, D. M. York, and W. Yang, J. Chem. Phys. **105**, 2744 (1996).
[38] S. L. Dixon and K. M. Merz, Jr., J. Chem. Phys. **104**, 6643 (1996).
[39] R. Haydock, *Solid State Physics* (Academic, New York, 1980),

Vol. 35, p. 215.
[40] C. A. White, B. G. Johnson, P. M. W. Gill, and M. Head-Gordon, Chem. Phys. Lett. **230**, 8 (1994).
[41] K. Ohno, Theor. Chim. Acta **2**, 219 (1964); G. Klopman, J. Am. Ceram. Soc. **86**, 4550 (1964).
[42] J. C. Slater and G. F. Koster, Phys. Rev. **94**, 1498 (1954).
[43] W. A. Harrison, *Electronic Structure and the Properties of Solids* (Freeman, New York, 1980).
[44] J. P. Perdew and Y. Wang, Phys. Rev. B **45**, 13244 (1992).
[45] G. Kresse and J. Hafner, Phys. Rev. B **47**, 558 (1993); G. Kresse and J. Furthmüller, *ibid.* **54**, 11169 (1996).
[46] P. E. Blöchl, Phys. Rev. B **50**, 17953 (1994); O. Bengone, M. Alouani, P. E. Blochl, and J. Hugel, *ibid.* **62**, 16392 (2000).
[47] D. R. Lide, *CRC Handbook of Chemistry and Physics*, 79th ed. (CRC, Boca Raton, 1998).
[48] K. P. Huber and G. Herzberg, *Molecular Spectra and Molecular Structure: Constants of Diatomic Molecules* (Van Nostrand, New York, 1979), Vol. IV.
[49] W. Vervisch, C. Mottet, and J. Goniakowski, Phys. Rev. B **65**, 245411 (2002).
[50] J. Goniakowski and C. Noguera, Interface Sci. **12**, 93 (2004).
[51] J. Goniakowski and C. Noguera, Phys. Rev. B **79**, 155433 (2009).
[52] T. P. Martin, Phys. Rep. **273**, 199 (1996).
[53] J. Goniakowski and C. Mottet, J. Cryst. Growth **275**, 29 (2005).